Temperature stabilized phase reference for MEMS based swept sources

Bart Johnson, Dean Tipple, Carlos Melendez, Ed Mallon, Walid Atia, et al.

Bart Johnson, Dean Tipple, Carlos Melendez, Ed Mallon, Walid Atia, Peter Whitney, "Temperature stabilized phase reference for MEMS based swept sources," Proc. SPIE 10867, Optical Coherence Tomography and Coherence Domain Optical Methods in Biomedicine XXIII, 108672Z (22 February 2019); doi: 10.1117/12.2508746

SPIE.

Event: SPIE BiOS, 2019, San Francisco, California, United States

Temperature stabilized phase reference for MEMS based swept sources

Bart Johnson, Dean Tipple, Carlos Melendez, Ed Mallon, Walid Atia, and Peter Whitney

Axsun Technologies, Billerica, MA, USA

ABSTRACT

MEMS tunable lasers are not inherently phase stable because Brownian motion and drive electronics noise make the starting wavelength of the sweep unstable with respect to the electrical sweep trigger. A typical solution to the problem is to use a fiber Bragg reflector wavelength trigger. That is a sub-optimal solution since environmental changes can move both the Bragg peak and the k-clock phase. We have packaged temperature controlled trigger and clock etalons in a butterfly package to solve this environmental problem. By making the wide FSR trigger etalon from silicon and the narrow FSR clock etalon from fused silica, the relative spectral positions of the trigger and clock can be adjusted through temperature control. The system has applications in background subtraction, phase-sensitive and Doppler sensing, synthetic aperture imaging, and long-term averaging to increase SNR. It can be used for direct hardware clocking of a DAQ board, as well as in a software resampling context.

Keywords: OCT, Optical Coherence Tomography, Swept source OCT, Phase stability

1. INTRODUCTION

Many optical coherence tomography (OCT) functions can benefit from a phase-stable swept laser. Vernier-tuned distributed Bragg reflector lasers are highly phase stable.[1] Spectral domain OCT systems are also phase stable.[2] MEMS tunable lasers, both short cavity lasers[3] and tunable VCSELs[4] are less so. The MEMS structures are so small that they are susceptible to Brownian motion and photon pressure effects[5] that can affect tuning. Also, simple electronic drive noise from high-bandwidth high-voltage drive circuits can contribute to this problem. The solution is to not rely on laser stability, but to measure the wavelengths in real time. Fiber Bragg grating sweep triggers partially solve this problem, but they are not stable over environmental changes.

We have packaged temperature controlled trigger and clock etalons in a butterfly package to solve this environmental problem. By making the wide free spectral range (FSR) trigger etalon from silicon and the narrow FSR clock etalon from fused silica, the relative spectral positions of the trigger and clock can be adjusted through temperature control. The stability is absolute and long term.

2. TEMPERATURE CONTROLLED ETALON MODULE

Two reflective etalons are incorporated in a temperature-controlled, hermetically sealed 14-pin butterfly package of Fig. 1(left). The idea is to use the coarse 82 GHz FSR etalon as an optical sweep trigger. Its FSR is larger than the typical laser jitter in Fig. 2(left) so there will be no mis-triggering. For direct electronic k-clocking of a DAQ board, it is important that the sweep trigger be placed between clock pulses to avoid ambiguity. This can be configured through temperature-tuning of the etalon module since the silicon and fused silica etalons have different temperature tuning rates as seen in Fig. 1(right). In our experiments, the clock etalon is a 6 mm length of fused silica with 20% reflective coatings.

A 1310 nm swept laser was used to test the module in Fig. 2. The oscilloscope traces of Fig. 2(center and right) show the laser jitter and how triggering on the coarse etalon compensates for the laser's sweep-to-sweep jitter.

Bart Johnson: bjohnson@axsun.com

Optical Coherence Tomography and Coherence Domain Optical Methods in Biomedicine XXIII
edited by James G. Fujimoto, Joseph A. Izatt, Proc. of SPIE Vol. 10867, 108672Z

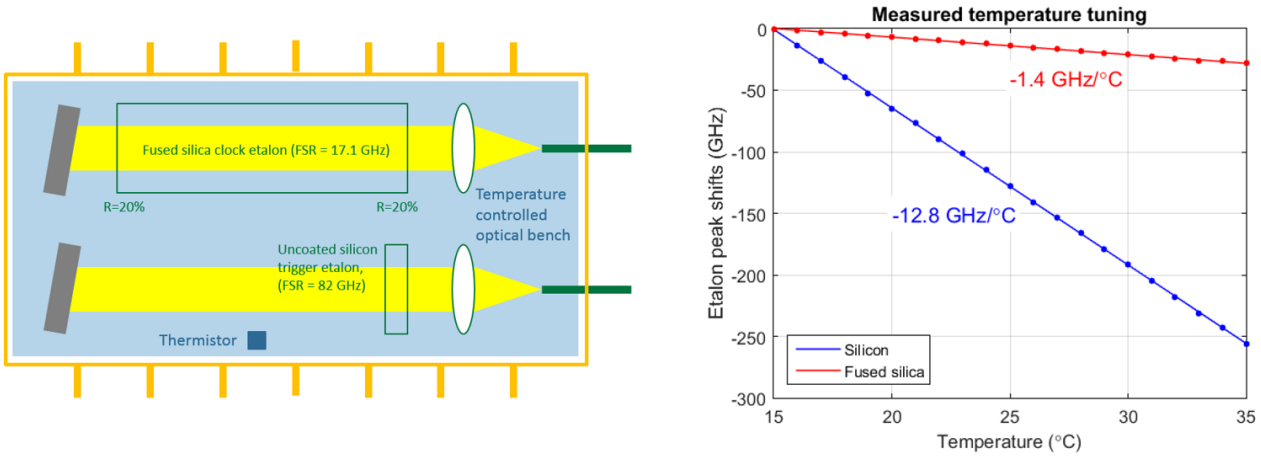

Figure 1. Diagram of the temperature-controlled clock/trigger etalon package (left). Temperature tuning rates of the silicon and fused silica etalons (right).

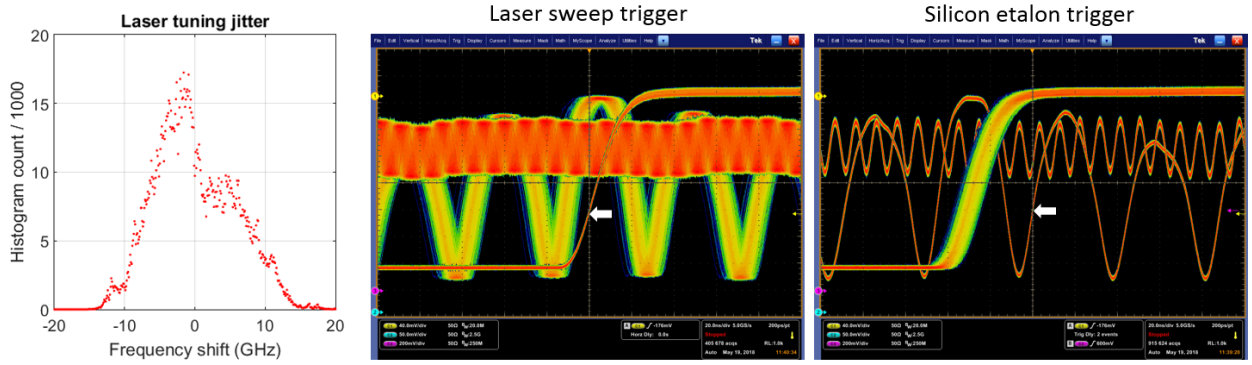

Figure 2. Histogram of the MEMS tunable laser jitter (left). Sweep trigger, optical trigger etalon, and clock etalon traces. Oscilloscope is triggered on the sweep trigger (center) and optical trigger (right).

3. HARDWARE CLOCKING

The temperature stabilized etalon module allows hardware clocking of a DAQ board. This is desirable for many real-time applications where software resampling may be a burdensome overhead. Long term stability is required for this application. Figure 3 shows how the engine sweep trigger allows optical triggering on the next trigger etalon transition. Phase stability is further increased by sampling on the next narrow FSR optical clock transition. Temperature adjustment of the etalon module's optical bench is used to place the optical trigger transition between the first clock pulse and its predecessor. This timing margin prevents false clocking and requires the stability that tight temperature control provides.

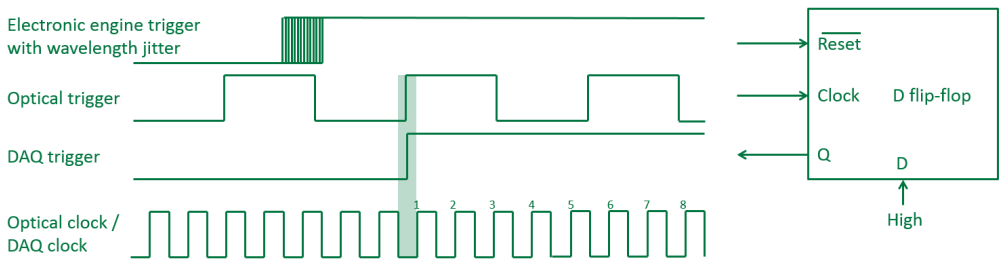

Figure 3. Waveforms for direct phase-sensitive sampling on a DAQ board.

4. STABILITY MEASUREMENTS

Long term stability of the reference etalons is ensured by active temperature control of the optical bench inside the butterfly package. These references are more stable than an etalon made from a 1-mm-thick etalon made from a microscope slide. The microscope slide is sensitive to room temperature as seen in Fig. 4. In Fig. 5, the 1350.41 nm water absorption line was monitored through a 1-meter air path. This reference is less sensitive to temperature than the etalon, and an RMS frequency uncertainty of 0.62 GHz was measured. The uncertainty is due to the relatively wide absorption line and the multi-mode nature of the swept source.

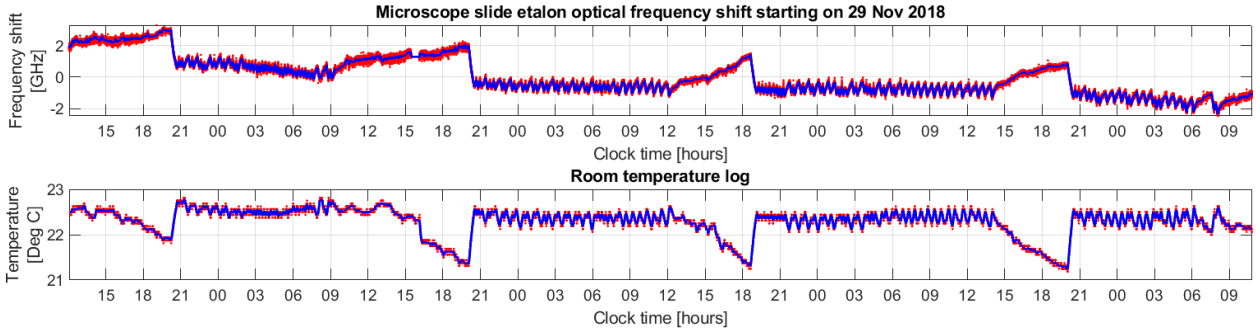

Figure 4. Plot of etalon peak shift as a function of time while the room temperature varied. Very high accuracy is obtained since this is a phase-sensitive measurement.

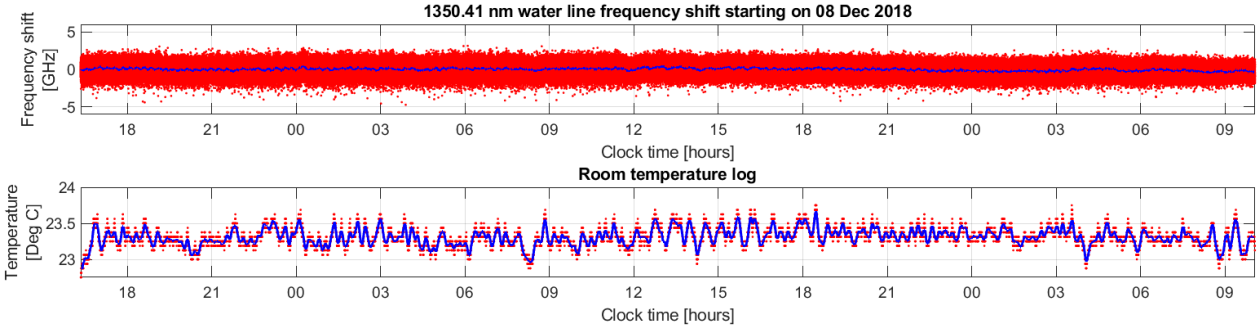

Figure 5. Tracking of the 1350.41 nm water absorption line over time. This is not a phase-sensitive measurement, so it has limited accuracy. On the other hand, it is a relatively temperature insensitive measurement.

5. PHASE-SENSITIVE DISPLACEMENT MEASUREMENT

The motion of a 3-inch audio speaker cone was studied by phase-sensitive OCT. To preserve the phase, a common path interferometer was set up where a reference reflection was provided by a microscope slide placed immediately in front of the speaker. The speaker was driven by a 5 Hz square wave and responded with a 300 Hz damped oscillation before settling into a step in displacement. The M-scan in the bottom plot of Fig. 6 shows that the motion is not well resolved by standard OCT. The native sweep has 950 samples and images out to a 4.38 mm Nyquist depth. The point spacing is 9.2 μm and the resolution for a Hann window is 13.3 μm. By zero padding the FFT, the point spacing was reduced 50$\times$ to 0.18 μm. Zero padding is of great value in locating peaks with finer resolution than the point-spread width but the method is still not as precise as phase-sensitive techniques where the signal phase at the reflection depth is converted to displacement by $\Delta z = (\Delta\phi/4\pi)\,\lambda$. This is illustrated in the top plot of Fig. 6, where the phase-sensitive measurement in red is compared to the gray dots from the peak-location method with 50$\times$ zero padding. The gray dots are spaced at 180 nm intervals, whereas the phase-sensitive measurement has an accuracy of better than 2 nm RMS.

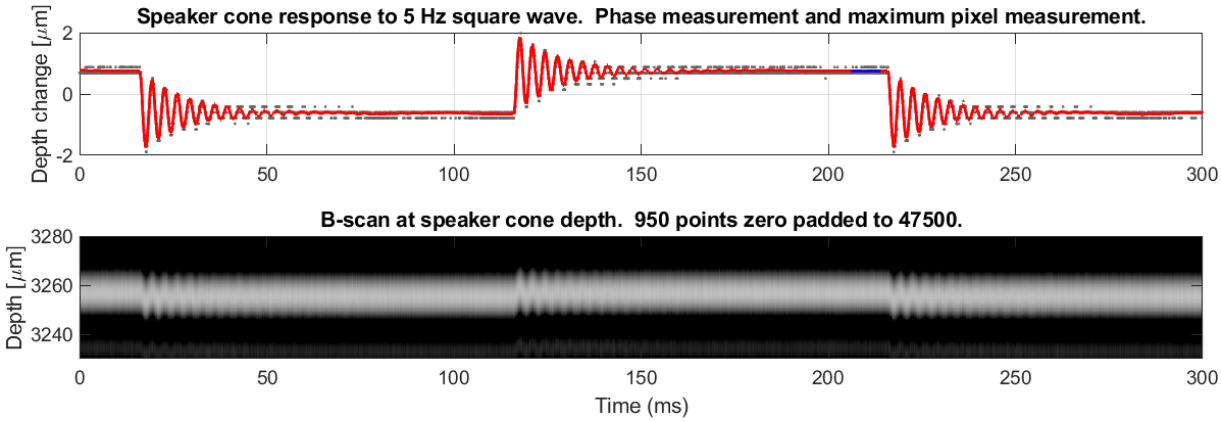

Figure 6. The top plot is a speaker cone displacement measurement in response to a 5 Hz square wave. The red curve is a phase-sensitive measurement and the gray dots are the maxima locations from the M-scan in the bottom plot.

This type of measurement is useful in studies of the inner ear.[6,7] The phase uncertainty, translated into physical motion, is dependent on the signal-to-noise ratio. A measurement of the spatial sensitivity is plotted vs. SNR in Fig. 7 along with the curve $\sigma_z = \lambda / \left(4\pi\sqrt{SNR}\right)$. The reason for the offset between the data and theoretical curve is not known at this point, but there is no obvious limitation of the system such as a floor to the sensitivity.

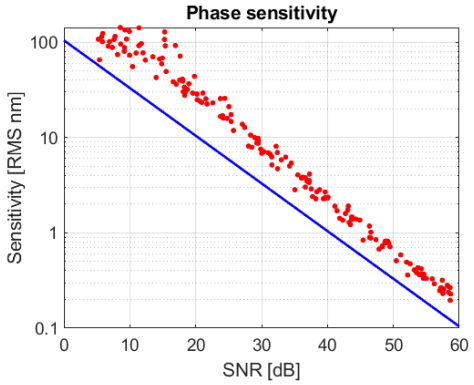

Figure 7. Displacement sensitivity vs. SNR for phase-sensitive imaging.

6. BACKGROUND SUBTRACTION

Figure 8 is a series of fingertip images plagued by horizontal fixed line artifacts that appear with and without a sample in the imaging beam. For demonstration purposes, the reference power was set at a very high level to raise the fixed pattern artifacts from the laser above the shot noise. Normally this would not be done. One deleterious effect of doing this is the vertical streaking from an SNR limit[8] brought about by simultaneously high sample and reference powers. There is also a lens reflection artifact deep in the center of the image. In the discussion that follows, we ignore the vertical streaking and the lens artifact, and focus our attention on the horizontal streaks associated with fixed pattern artifacts.

The image series (a-c) was taken with a phase-stable optical trigger and direct hardware clocking of the DAQ board. Series (d-f) was taken with the normal engine trigger (not phase-stable). In both series, a raw image was taken (a) and (d), and another background image without the finger in place was taken. In (b) and (e), the two-dimensional foreground and background images were simply subtracted. This raises the noise floor since the foreground and background noises are added together. In (c) and (f), the 4000 background lines are averaged

before subtracting from the image. This solves the added noise problem. Comparison of (b) to (e) and (c) to (f) shows the value of phase stability in background subtraction. Even very deep fixed patterns can be effectively eliminated, as seen in images (b) and (c).

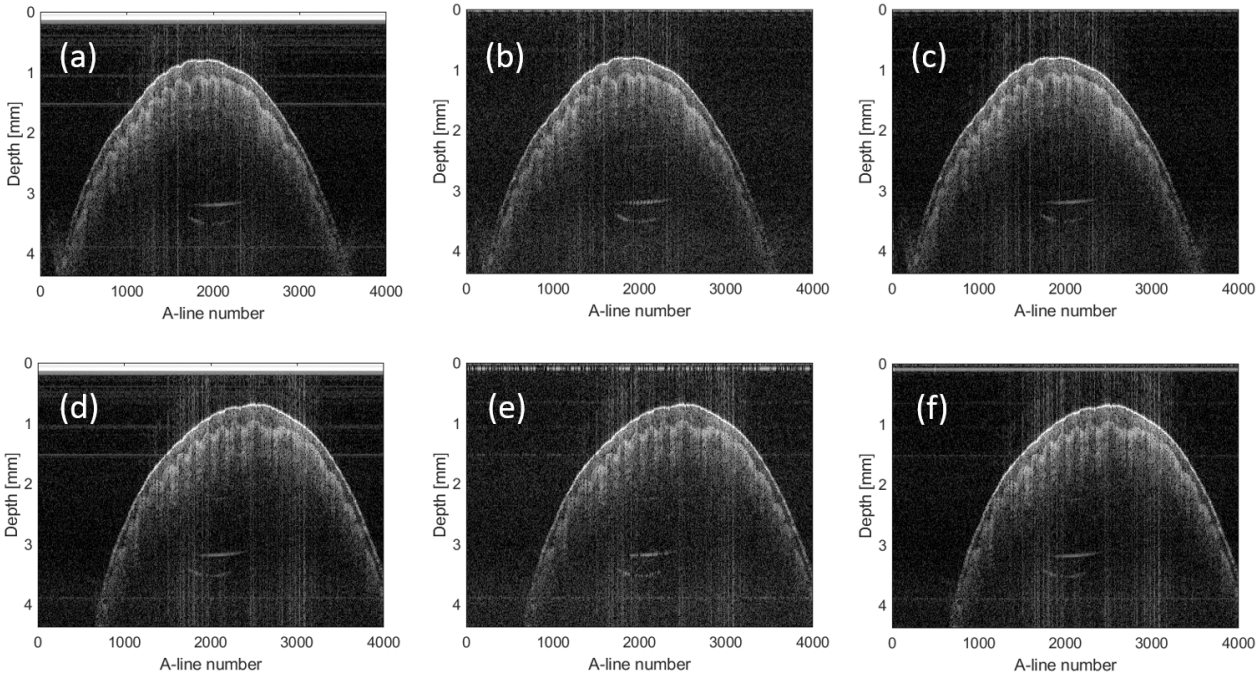

Figure 8. Figure (a) is a raw image with two types (b) and (c) of phase-sensitive background subtraction. Images (d), (e), (f) are a similar series without the phase-stable optical sweep trigger.

7. PHASE SENSITIVE AVERAGING

There are different types of averaging that can be used in OCT.[9] Averaging the post-FFT electronic power traces, throwing away the phase, can be used to get a better estimate of the noise floor. There the signal is preserved but the noise floor hash is smoothed allowing a better estimate for the single-sweep SNR. Averaging traces in the time domain, or equivalently in the frequency domain if the phase information is retained (complex averaging) can improve the SNR at the expense of averaging time. Phase stability of the swept source is essential for this to take place. Otherwise the signals do not add coherently to maintain the "signal" portion of the signal-to-noise.

```
% Samples_2D is a sample array, N samples x NLines A-lines.
% The Window_2D array is the same size (Hann window).
% NComplexAverage is the number of A-lines averaged retaining the phase informaton.
% These groups numbering N/NComplexAverage are further averaged without phase
% Fourier transformed variable are capitalized
N = size(Samples_2D,1);
NLines = size(Samples_2D,2);
Windowed_Samples_2D = Samples_2D.*Window_2D;
Windowed_Samples_3D = reshape(Windowed_Samples_2D,N,NComplexAverage,NLines/NComplexAverage);
WINDOWED_SAMPLES_3D = fft(Windowed_Samples_3D);
COMPLEX_AVERAGE_POWER = abs(  mean(WINDOWED_SAMPLES_3D(1:N/2,:,:),2)  ).^2;
TOTAL_MEAN_POWER = mean(COMPLEX_AVERAGE_POWER,3);
dB = 10*log10(TOTAL_MEAN_POWER);
```

Figure 9. MATLAB code used to compute the averaged traces.

We use a tunable SLED[8] as a source since it has well characterized, uniform noise. We probed a solid etalon in a common path configuration since we need a signal that is phase stable over an extended period of time.

Consequently, there is no RIN subtraction from balanced detection. The mathematical processing is outlined by the Matlab code in Fig. 9. This demonstration was done by software resampling based on the phase-stable clock, rather than direct hardware clocking. We have also done this experiment with a laser source, although the complex averaging tends to reach a noise reduction limit determined by laser artifacts.

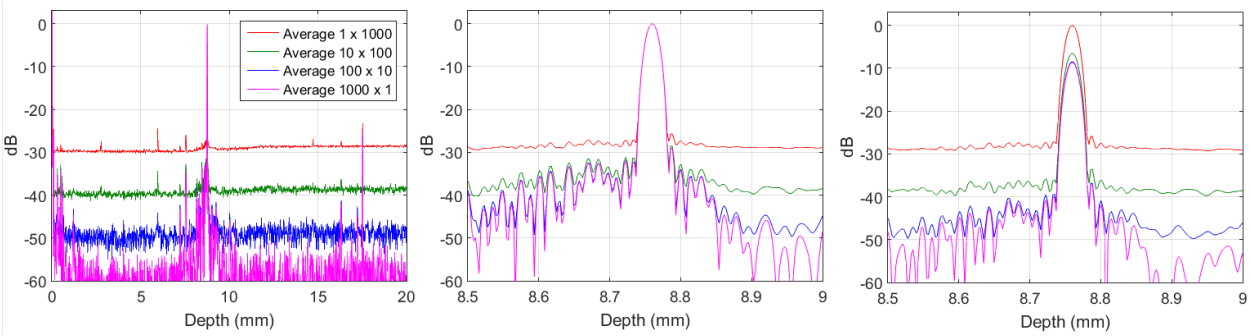

Figure 10. Four averaging experiments (left) and expanded views (center and right). With phase-correction (center) and without (right).

Complex averaging reduces the noise floor by 10 dB for every factor of 10 averages as seen in Fig. 10(left). The number of complex averages times the number of power (no phase) averages is 1000, the number of A-lines collected. The hash becomes greater for the higher number of complex averages because there are fewer power averages. Figure 10(center) shows the etalon peak for optically-triggered phase stable sampling, compared with that of Fig. 10(right) using just the engine sweep trigger as a reference. Phase stability is required to keep the signal from degrading. The noise will average down in any case.

High SNR is provided by longer averaging times. One way to achieve this is to sweep slower and integrate longer. However, many OCT swept sources cannot be run at slow rates. In those cases, phase-stable complex averaging can be applied.

8. SUMMARY

Phase stable swept sources have applications in OCT including background subtraction, phase-sensitive and Doppler sensing, SNR boosting through phase-sensitive averaging, and synthetic aperture imaging.[10] Such a source could be absolutely calibrated for high-speed gas-line spectroscopy. This source can be utilized in both hardware clocking and software resampling contexts. Long term phase stability is possible with this system, making MEMS driven sources such as short cavity lasers and tunable VCSELs have comparable phase stability to akinetic sources and spectral domain systems.

REFERENCES

[1] Chen, Z., Liu, M., Minneman, M., Ginner, L., Hoover, E., Sattmann, H., Bonesi, M., Drexler, W., and Leitgeb, R. A., "Phase-stable swept source OCT angiography in human skin using an akinetic source," *Biomed. Opt. Express* **7**, 3032–3048 (Aug 2016).

[2] Choma, M. A., Ellerbee, A. K., Yang, C., Creazzo, T. L., and Izatt, J. A., "Spectral-domain phase microscopy," *Opt. Lett.* **30**, 1162–1164 (May 2005).

[3] Kuznetsov, M., Atia, W., Johnson, B., and Flanders, D. C., "Compact ultrafast reflective Fabry-Perot tunable lasers for OCT imaging applications," *Proc. of SPIE* **7554**, 75541F–1 (2010).

[4] Choi, W., Potsaid, B., Jayaraman, V., Baumann, B., Grulkowski, I., Liu, J., Lu, C., Cable, A., Huang, D., Duker, J., and Fujimoto, J., "Phase-sensitive swept-source optical coherence tomography imaging of the human retina with a vertical cavity surface-emitting laser light source," *Optics Letters* **38**, 338–340 (2013).

[5] Tucker, R. S., Baney, D. M., Sorin, W. V., and Flory, C. A., "Thermal noise and radiation pressure in MEMS Fabry-Perot tunable filters and lasers," *IEEE J. of Selected Topics in Quantum Electronics* **8**, 88–97 (2002).

[6] Ramier, A., Rosowski, J., and Yun, S.-H., "Optical coherence tomography for imaging the middle and inner ears: A technical review," *AIP Conference Proceedings* **1965**, 020001/1–12 (2018).

[7] Applegate, B., Park, J., Carbajal, E., and Oghalai, J., "Phase-sensitive optical coherence tomography-based vibrometry using a highly phasestable akinetic swept laser source," *AIP Conference Proceedings* **1703**, 040001/1–5 (2015).

[8] Johnson, B., Atia, W., Flanders, D. C., Kuznetsov, M., Goldberg, B. D., Kemp, N., and Whitney, P., "SNR of swept SLEDs and swept lasers for OCT," *Opt. Express* **24**, 11174–11186 (May 2016).

[9] Szkulmowski, M. and Wojtkowski, M., "Averaging techniques for OCT imaging," *Opt. Express* **21**, 9757–9773 (Apr 2013).

[10] Xu, Y., Liu, Y.-Z., Boppart, S. A., and Carney, P. S., "Automated interferometric synthetic aperture microscopy and computational adaptive optics for improved optical coherence tomography," *Appl. Opt.* **55**, 2034–2041 (Mar 2016).